

Controlling synchronous patterns in complex networksWeijie Lin,^{1,2} Huawei Fan,² Ying Wang,² Heping Ying,¹ and Xingang Wang^{2,3,*}¹*Department of Physics, Zhejiang University, Hangzhou 310027, China*²*School of Physics and Information Technology, Shaanxi Normal University, Xi'an 710062, China*³*Institute of Theoretical & Computational Physics, Shaanxi Normal University, Xi'an 710062, China*

(Received 9 November 2015; revised manuscript received 30 March 2016; published 18 April 2016)

Although the set of permutation symmetries of a complex network could be very large, few of them give rise to stable synchronous patterns. Here we present a general framework and develop techniques for controlling synchronization patterns in complex network of coupled chaotic oscillators. Specifically, according to the network permutation symmetry, we design a small-size and weighted network, namely the control network, and use it to control the large-size complex network by means of pinning coupling. We argue mathematically that for *any* of the network symmetries, there always exists a critical pinning strength beyond which the unstable synchronous pattern associated to this symmetry can be stabilized. The feasibility of the control method is verified by numerical simulations of both artificial and real-world networks and demonstrated experimentally in systems of coupled chaotic circuits. Our studies show the controllability of synchronous patterns in complex networks of coupled chaotic oscillators.

DOI: [10.1103/PhysRevE.93.042209](https://doi.org/10.1103/PhysRevE.93.042209)**I. INTRODUCTION**

Synchronous behaviors are commonly observed in natural and man-made systems and are widely recognized as important to the system functionality and operations [1–3]. In theoretical studies, a popular approach to investigating synchronization is to couple an ensemble of dynamical oscillators, and one of the central tasks is to find the necessary conditions under which the whole system is globally synchronized, or, in some circumstances, the onset of synchronization occurs [4,5]. From the viewpoint of synchronization transition, the onset of synchronization and global synchronization stand, respectively, as the starting and ending points, which are mostly concerned for the physical and engineering systems [6–8]. However, for the neuronal and biological systems, experimental evidences have shown that the system dynamics is normally lying somewhere in between [9]. Specifically, the oscillators are found to be organized into different clusters, with the motions of the oscillators being highly correlated if they belong to the same cluster, and loosely or not correlated if they belong to different clusters [10]. Stimulated by these experimental observations, in the past decades considerable attentions have been given to the study of cluster (partial, group) synchronization in systems of coupled oscillators [11–23].

Recently, with the discoveries of the small-world and scale-free properties in many realistic systems [24,25], the study of complex network synchronization has received broad interest [26–29]. While most of the synchronization phenomena observed previously in regular networks have been successfully reproduced in complex networks, it remains a challenge to generate cluster synchronization in complex networks, due to the presence of random connections [30–32]. By the bifurcation theory of pattern formation, the generation of cluster synchronization relies strictly on the network symmetry [33–35], which, at the first glance, is absent in complex networks. In recent years, with the in-depth studies on the

relationship between network structure and synchronization, breakthroughs have been made on this topic, from which arises the new interest of studying cluster synchronization in complex networks [15–23]. In particular, using the technique of computational group theory [36], in a recent study Pecora *et al.* are able to identify all the permutation symmetries of a complex network and, based on the method of eigenvalue analysis, predict the stable synchronous patterns that can be generated from the random initial conditions [22]. This finding extends significantly the conventional understanding on cluster synchronization, and, more significantly, points out the “key” to exploring cluster synchronization in complex networks: the network permutation symmetry [37]. Although the set of symmetries of a complex network is generally huge, their corresponding synchronous patterns are mostly unstable, making cluster synchronization rarely observed in complex networks [15–22]. Concerning the important implications of cluster synchronization to the security and functioning of many realistic networks, a natural question therefore would be: *Is it possible to stabilize the unstable synchronous patterns in complex networks by some control methods and techniques?*

In the present work, we are going to argue and demonstrate that, by a small-size control network designed according to the network permutation symmetry, it is indeed possible to control a large-size complex network to the synchronous pattern supported by the network symmetry. This finding sheds new light on the synchronous behaviors of complex networks and would be helpful to our understanding on the functioning of neuronal complex systems (e.g., the functioning of the vertebrate mesencephalic ventral tegmentum, in which a collection of dopamine (DA)-expressing neurons in the midbrain DA complex are self-organized into dynamical patterns according to the functional sectors while each sector is used to coordinate the collective dynamical behavior of a specific functional-anatomical macrosystem of the basal forebrain [38,39]) and be instructive to the design of modern techniques for controlling dynamical patterns in complex engineering networks (e.g., the control of the international (global) power-grid, in which units (power stations) within a

*wangxg@snnu.edu.cn

nation are synchronized to the same frequency and phase, but may be different among the nations [40,41]).

The rest of the paper is organized as follows. In Sec. II, we shall present our model of networked oscillators and introduce the new control method. In Sec. III, based on the method of eigenvalue analysis, we shall conduct a detail analysis on the stability of the synchronous patterns and derive explicitly the necessary conditions for inducing and controlling the synchronous patterns. In Sec. IV, we shall apply the proposed control method to different network models, including the numerical studies of artificial and real-world networks, and the experimental demonstration of networked electronic circuits. Discussions and conclusion shall be given in Sec. V.

II. MODEL AND CONTROL METHOD

Our model of networked chaotic oscillators reads [42]

$$\dot{\mathbf{x}}_i = \mathbf{F}(\mathbf{x}_i) + \varepsilon \sum_{j=1}^N w_{ij} \mathbf{H}(\mathbf{x}_j), \quad (1)$$

with $i, j = 1, 2, \dots, N$ the oscillator (node) indices and N the network size. \mathbf{x}_i is the state vector associated with the i th oscillator, and $\mathbf{F}(\mathbf{x})$ describes the dynamics of the oscillators in the isolated form, which, for the sake of simplicity, is set as identical in the network. ε is the uniform coupling strength. $\mathbf{H}(\mathbf{x})$ denotes the coupling function. The coupling relationship among the oscillators, i.e., the network topological structure, is captured by the matrix $\mathbf{W} = \{w_{ij}\}$, with $\varepsilon w_{ij} = \varepsilon w_{ji} > 0$ the strength that node j is coupled to node i . If there is no link between nodes i and j , $w_{ij} = 0$. The diagonal elements are set as $w_{ii} = -\sum_j w_{ij}$, so as to make \mathbf{W} a Laplacian matrix. Equation (1), or its equivalent forms, describes the dynamics of a large variety of spatiotemporal systems and has been employed as one of the standard models in exploring the synchronization behaviors of coupled oscillators [42].

Before presenting our new control method, we first describe how to group the network nodes into clusters according to the network symmetries [22]. Let i and j be a pair of nodes in the network whose permutation (exchange) does not change the system dynamical equations [Eq. (1)], we call (i, j) a symmetric pair and characterize it by the permutation symmetry g_{ij} . Scanning over all the node pairs in the network, we are able to identify the whole set of permutation symmetries $\{g_{ij}\}$, which forms the symmetry group G . Each symmetry g can be further characterized by a permutation matrix \mathbf{R}_g , with $r_{ij} = r_{ji} = 1$ if (i, j) is a symmetric pair, and $r_{ij} = 0$ otherwise. \mathbf{R}_g is commutative with the coupling matrix, i.e., $\mathbf{R}_g \mathbf{W} = \mathbf{W} \mathbf{R}_g$, and, after operating on \mathbf{W} , it only exchanges the indices of nodes i and j . The set of permutation symmetries of a (unweighted) complex network could be large and difficult to be identified [22], but can be obtained from \mathbf{W} by the technique of computational group theory [36]. (We note that for large-scale complex network of random link weight or nonidentical local dynamics, unless the link weight and local dynamics are specially arranged, it is hard to find any symmetry in the network.) Having obtained the symmetry group G , we then can partition the network nodes into clusters according to the permutation orbits, i.e., the subset of nodes permuting among one another by the permutation operations

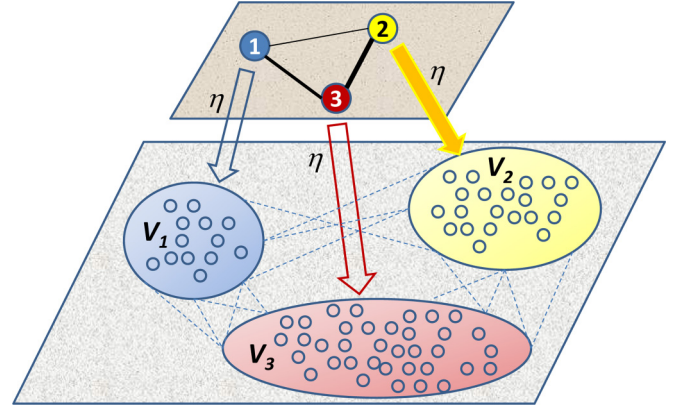


FIG. 1. A schematic plot of the control method. The lower layer represents the network to be controlled, which consists of $M = 3$ clusters. Nodes within each cluster are permuting among one another. The upper layer represents the control network, which consists of three controllers. Each controller in the control network is coupled unidirectionally to all nodes in the cluster associated to it.

are grouped into the same cluster. In such a way, the network nodes are grouped into a small number of clusters $\{V_l\}$ (see the lower layer in Fig. 1 for illustration), with V_l the set of nodes belonging to cluster l . The clusters provide the topological basis for the formation of synchronous patterns, yet the patterns might not be stable, due to either the dynamical or topological instability (more details to be described below).

We now present our control method for stabilizing the synchronous patterns. First, a small-size, weighted network is designed according to the cluster information (the upper layer in Fig. 1). The size of the control network is identical to the number of clusters in the original network, and the connections of the control network are weighted as

$$c_{lm} = \sum_{i \in V_l} \sum_{j \in V_m} w_{ij} / n_l, \quad (2)$$

with $l, m = 1, \dots, M$ the cluster indices and M the size of the control network (also the number of clusters of the original network). n_l represents the size of the l th cluster, and V_l denotes the set of nodes belonging to cluster l . Physically, c_{lm} can be understood as the average coupling strength that a node in cluster l is received from cluster m . In general, we have $c_{lm} \neq c_{ml}$, i.e., links in the control network are also directed. The dynamics of the control network is still governed by Eq. (1), except that the coupling matrix is defined by Eq. (2) and the network size is changed to M . To implement the control, we couple *unidirectionally* each node (controller) in the control network to all nodes in the cluster associated to it. More specifically, the l th controller is coupled to all nodes in V_l , with l ranging from 1 to M . (A schematic plot of the control method is presented in Fig. 1.)

Unifying the control and original networks into a large-size network, the dynamics of the enlarged network reads

$$\dot{\mathbf{x}}_l = \mathbf{F}(\mathbf{x}_l) + \sum_{m=1}^M c_{lm} \mathbf{H}(\mathbf{x}_m), \quad (3)$$

$$\dot{\mathbf{x}}_i = \mathbf{F}(\mathbf{x}_i) + \varepsilon \sum_{j=1}^N w_{ij} \mathbf{H}(\mathbf{x}_j) + \eta \varepsilon \sum_{l=1}^M \delta_{il} \mathbf{H}(\mathbf{x}_l), \quad (4)$$

where Eqs. (3) and (4) describes, respectively, the dynamics of the control and original networks. We set $c_{il} = -\sum_m c_{lm}$ in Eq. (3), so as to make \mathbf{C} a Laplacian matrix. In Eq. (4), η denotes the normalized control (pinning) strength, and δ is the delta function: $\delta_{il} = 1$ if $i \in V_l$, and $\delta_{il} = 0$ otherwise. For the system dynamics described by Eqs. (3) and (4), the specific questions we are interested in are: Can we stabilize the unstable synchronous patterns by the control network designed as such? If yes, what is the necessary controlling strength?

III. THEORETICAL ANALYSIS

Due to the network symmetry, the topological clusters provide naturally a solution for the synchronous pattern. To be specific, if we set the initial conditions of all nodes inside the same cluster to be identical, then during the process of the system evolution, these nodes will be always synchronized whatever the coupling strength. This is because that nodes within the same cluster are surrounded by the same set of neighboring nodes, and thus are perturbed by the same coupling signals throughout the evolution. The synchronous pattern defined as such, however, is generally unstable. Let $\mathbf{s}_l(t)$ be the synchronous manifold of the l th cluster and $\delta\mathbf{x}_i = \mathbf{x}_i - \mathbf{s}_l$ be the infinitesimal perturbations added onto oscillator i , then whether the oscillators inside cluster l are synchronizable is basically determined by the following set of variational equations:

$$\begin{aligned} \delta\dot{\mathbf{x}}_i &= D\mathbf{F}(\mathbf{s}_l)\delta\mathbf{x}_i + \varepsilon \sum_{j \in V_l} w_{ij} D\mathbf{H}(\mathbf{s}_l)\delta\mathbf{x}_j \\ &+ \varepsilon \sum_{m \neq l} \sum_{j' \in V_m} w_{ij'} [D\mathbf{H}(\mathbf{s}_m)\delta\mathbf{x}_{j'} - D\mathbf{H}(\mathbf{s}_l)\delta\mathbf{x}_i], \end{aligned} \quad (5)$$

with $i, j = 1, \dots, n_l$ the oscillators belonging to cluster l . \mathbf{s}_m denotes the synchronous manifold of the m th cluster, and $\delta\mathbf{x}_{j'} = \mathbf{x}_{j'} - \mathbf{s}_m$ (with $j' \in V_m$) represents the perturbations of the j' th oscillator from \mathbf{s}_m . $D\mathbf{F}(\mathbf{s}_l)$ and $D\mathbf{H}(\mathbf{s}_l)$ are the Jacobin matrices evaluated on \mathbf{s}_l . In Eq. (5), the second term on the righthand side represents the coupling signals that oscillator i receives from oscillators within the same cluster, and the third term represents the coupling signals that i receives from oscillators in other clusters ($m \neq l$). For the synchronous pattern to be stable, the necessary condition is that $\delta\mathbf{x}_i$ approaches 0 with time for all oscillators in the network. (Please note that this condition is different from that of global synchronization, where all the oscillator trajectories are required to be converged to the same manifold. Here, oscillators in different clusters are converged to different manifolds.)

Denoting $\Delta\mathbf{X} = [\Delta\mathbf{X}_1, \Delta\mathbf{X}_2, \dots, \Delta\mathbf{X}_M]^T$ as the network perturbation vector, with $\Delta\mathbf{X}_l = [\delta\mathbf{x}_{l,1}, \delta\mathbf{x}_{l,2}, \dots, \delta\mathbf{x}_{l,n_l}]^T$ the perturbation vector associated to cluster l , then the variational equations of Eq. (5) can be rewritten as

$$\Delta\dot{\mathbf{X}} = \left[\sum_{l=1}^M \mathbf{E}^l \otimes D\mathbf{F}(\mathbf{s}_l) + \varepsilon \mathbf{W} \sum_{l=1}^M \mathbf{E}^l \otimes D\mathbf{H}(\mathbf{s}_l) \right] \Delta\mathbf{X}. \quad (6)$$

Here, \mathbf{E}^l is an N -dimensional diagonal matrix, with $E_{ii}^l = 1$ if $i \in V_l$, and $E_{ii}^l = 0$ otherwise. To analyze the stability of the synchronous pattern, the key question is how to decouple the

clusters from each other (so that the stability of the clusters can be treated individually). This can be accomplished by transforming the variational equations into the mode space spanned by the eigenvectors of the network permutation matrix, with the details as follows. (The mathematical treatment to be described below is modified from Ref. [22], but is more efficient and easier to operate. In Ref. [22], the authors employ the irreducible representations to diagonalize the transverse space of the coupling matrix, which relies on a specially designed code and is computationally costly. In our treatment, we first transform the coupling matrix to the blocked diagonal form and then diagonalize the transverse blocks individually, which can be done by the conventional routine and is much efficient in simulation.) First, based on the network symmetry, we can construct the network permutation matrix \mathbf{R} , with $r_{ij} = r_{ji} = 1$ if nodes i and j belong to the same cluster, and $r_{ij} = r_{ji} = 0$ otherwise. Second, by finding the eigenvectors of \mathbf{R} , we can construct the transformation matrix \mathbf{T} , such that the transformed matrix $\mathbf{R}' = \mathbf{T}^{-1}\mathbf{R}\mathbf{T}$ is diagonal. Finally, transforming Eq. (6) to the mode space of \mathbf{T} , we obtain

$$\Delta\dot{\mathbf{Y}} = \left[\sum_{l=1}^M \mathbf{E}^l \otimes D\mathbf{F}(\mathbf{s}_l) + \varepsilon \mathbf{G} \sum_{l=1}^M \mathbf{E}^l \otimes D\mathbf{H}(\mathbf{s}_l) \right] \Delta\mathbf{Y}, \quad (7)$$

with $\Delta\mathbf{Y} = \mathbf{T}^{-1}\Delta\mathbf{X}$ and $\mathbf{G} = \mathbf{T}^{-1}\mathbf{W}\mathbf{T}$. Particularly, in the mode space the coupling matrix \mathbf{G} has the blocked form

$$\mathbf{G} = \begin{pmatrix} \mathbf{B} & \mathbf{0} \\ \mathbf{0} & \mathbf{D} \end{pmatrix}, \quad (8)$$

where $\mathbf{B} = \bigoplus_{l=1}^M \mathbf{B}_l$, with \mathbf{B}_l an $(n_l - 1)$ -dimensional matrix. As \mathbf{B}_l characterizes the motions transverse to the synchronous manifold \mathbf{s}_l [21], we name the associated space the transverse subspace of cluster l . The M -dimensional matrix \mathbf{D} , on the other hand, characterizes the motions parallel to the synchronous manifolds $\{\mathbf{s}_l\}$, we thus name the associated space the synchronous space. Please note that because \mathbf{W} and \mathbf{G} are similar matrices, they have the same set of eigenvalues. In particular, the null eigenvalue, which characterizes the manifold of the global synchronization, belongs to \mathbf{D} . The significance of this transformation is that the eigenvalues are now divided into two distinct groups: one for the transverse subspaces (associated to the matrix \mathbf{B}) and one for the synchronous subspace (associated to the matrix \mathbf{D}). More importantly, the transverse subspaces of the clusters are *decoupled* from each other, so that the synchronization stability of the clusters can be analyzed separately.

Having decoupled the transverse subspaces, the stability of the l th cluster now is determined by the equation

$$\Delta\dot{\mathbf{Y}}_l = [\mathbf{I}_{n_l} D\mathbf{F}(\mathbf{s}_l) + \varepsilon \mathbf{B}_l D\mathbf{H}(\mathbf{s}_l)] \Delta\mathbf{Y}_l, \quad (9)$$

with $n'_l = n_l - 1$, $\Delta\mathbf{Y}_l = [\delta\mathbf{y}_{l,1}, \delta\mathbf{y}_{l,2}, \dots, \delta\mathbf{y}_{l,n'_l}]^T$ the transverse modes of \mathbf{s}_l , and $\mathbf{I}_{n'_l}$ the n'_l -dimensional identity matrix. To make the l th cluster synchronizable, $\delta\mathbf{y}_{l,i}$ should be damping with time for all the n'_l transverse modes. Treating each cluster as an isolated network, this is essentially a problem of global synchronization, which can be analyzed by the method of master stability function (MSF) [43–45]. Specifically, projecting $\Delta\mathbf{Y}_l$ into the eigenspace of \mathbf{B}_l (spanned by the eigenvectors of \mathbf{B}_l), then Eq. (9) can be transformed into

n'_l decoupled equations,

$$\delta \dot{\mathbf{y}}_{l,i} = [\mathbf{D}\mathbf{F}(\mathbf{s}_l) + \varepsilon \lambda_{l,i}^t \mathbf{D}\mathbf{H}(\mathbf{s}_l)] \delta \mathbf{y}_{l,i}, \quad (10)$$

with $i \in [1, n'_l]$ and $0 > \lambda_{l,1}^t \geq \lambda_{l,2}^t \geq \dots \geq \lambda_{l,n'_l}^t$ the eigenvalues of \mathbf{B}_l . Let $\Lambda_{l,i}$ be the largest Lyapunov exponent calculated from Eq. (10), then whether $\delta \mathbf{y}_{l,i}$ is damping with time is determined by the sign of $\Lambda_{l,i}$: the mode is stable if $\Lambda_{l,i} < 0$, and is unstable if $\Lambda_{l,i} > 0$. Defining $\sigma \equiv -\varepsilon \lambda^t$, by solving Eq. (10) numerically we can obtain the function $\Lambda = \Lambda(\sigma)$. Previous studies of MSF have shown that for the typical nonlinear oscillators [43–45], Λ is negative when σ is larger to a critical threshold σ_c , with σ_c a parameter dependent of both the oscillator dynamics and coupling function. (Another typical situation is that Λ is negative in a bounded region (σ_1, σ_2)). Our theoretical analysis, as well as the control method, can be generalized to this situation straightforwardly. It should be noted that for such a case, the stability of the l synchronous cluster is jointly determined by the modes $\lambda_{l,1}$ and λ_{l,n'_l} , rendering it relatively difficult to be generated.) As such, to keep the l th cluster synchronizable, the necessary condition becomes $\sigma_{l,i} > \sigma_c$ for $i = 1, 2, \dots, n'_l$; and, to keep the synchronous pattern stable, this condition should be satisfied for all the M clusters.

To better describe the mechanism of cluster synchronization, we plot Fig. 2, which shows schematically how the transverse modes are stabilized as the coupling (controlling) strength is increased. In Fig. 2, each (large) filled circle represents the transverse modes, $\{\delta \mathbf{y}_l\}$, of a specific cluster, and the dotted empty circles represent the synchronous modes

(manifolds), $\{\mathbf{s}_l\}$. Let $0 = \lambda_1^s > \lambda_2^s \geq \dots \geq \lambda_M^s$ be the eigenvalues of \mathbf{D} and denote λ_{\min} as the largest eigenvalue among all the transverse modes, i.e., $\lambda_{\min} = \min\{|\lambda_{l,1}^t|, l = 1, \dots, M\}$, then the scenario of cluster synchronization is dependent on the relationship between $|\lambda_2^s|$ and λ_{\min} . If $|\lambda_2^s| < \lambda_{\min}$ [as the case shown in Fig. 2(a1)], cluster synchronization can be achieved by varying the coupling strength ε . More specifically, given that all the transverse modes are staying in the stable region and, in the meantime, at least one of the synchronous modes is staying in the unstable region, cluster synchronization will be generated. This requirement thus gives the range for generating stable synchronous pattern, $\varepsilon \in (\varepsilon_1, \varepsilon_2)$, with $\varepsilon_1 = \sigma_c / \lambda_{\min}$ and $\varepsilon_2 = \sigma_c / |\lambda_2^s|$. On the other hand, if $|\lambda_2^s| > \lambda_{\min}$ [as the case shown in Fig. 2(b1)], cluster synchronization cannot be generated by varying ε . This is because that when the most unstable transverse mode, λ_{\min} , is shifted into the stable region, all the nontrivial synchronous modes will be already in the stable region, resulting in global synchronization instead of cluster synchronization. As λ_2^s and λ_{\min} are determined by only the network structure, for the latter cluster synchronization cannot be generated by varying the coupling strength, i.e., the synchronous pattern is topologically unstable.

We proceed to analyze the stability of the synchronous pattern when the control network is activated. Regarding the original and control networks as two connected parts of an enlarged network, then the control problem is essentially a problem of network synchronization, except that the synchronous manifolds are *predefined* by the control network. Similar to the analysis presented above for cluster

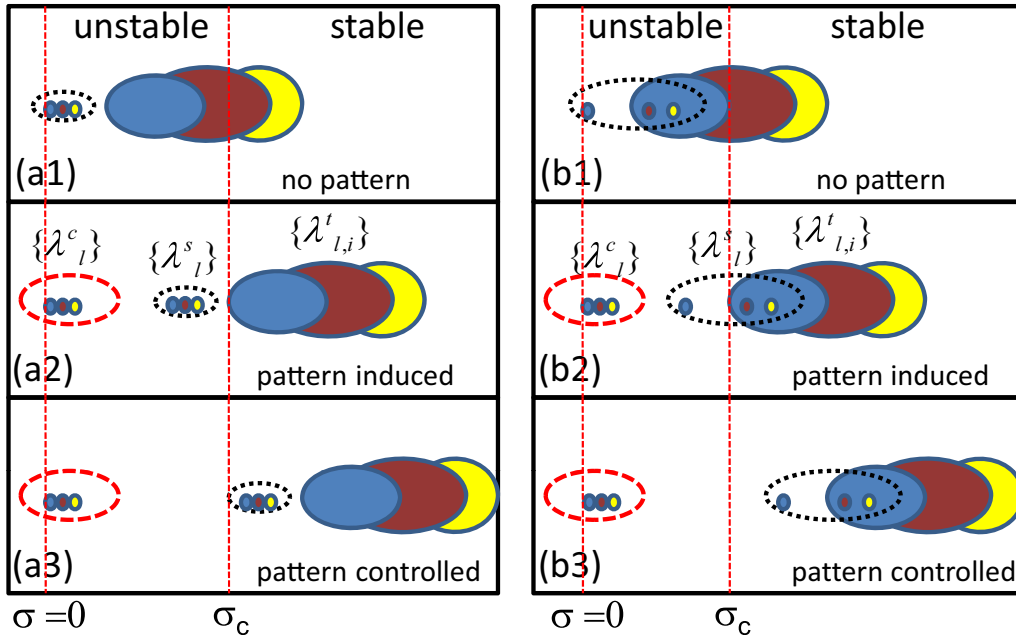


FIG. 2. Schematic plots showing the mechanism of cluster synchronization for the cases of dynamically unstable (a1–a3) and topologically unstable (b1–b3) networks. (a1) Without the control network, the distribution of the eigenmodes in the parameter space of σ . As some transverse modes are staying in the unstable regime, the synchronous pattern is unstable. (a2) With the control network, synchronous pattern is induced when the controlling strength $\eta > \eta_1$. (a3) $\eta > \eta_2$, the synchronous pattern is controlled to the state of the control network. (b1) Without the control network, the distribution of the eigenmodes. Cluster synchronization cannot be generated by varying the coupling strength, due to the topological instability. (b2) Cluster synchronization is induced by the control network when $\eta > \eta_1$. (b3) The synchronous pattern is controlled when $\eta > \eta_2$. Filled colored circles: the transverse modes associated to different clusters. Dotted empty circles (black): the synchronous modes $\{\mathbf{s}_l\}$. Dashed empty circles (red): the controlling modes. Modes are stable in the region of $\sigma > \sigma_c$.

synchronization, for the control problem we can still decouple the transverse modes by transforming the variational equations into the mode space of the permutation matrix of the enlarged network (which actually is identical to that of the original network, as the controllers are coupled to the oscillators in the one-way fashion). After the transformation, the coupling matrix has the blocked form

$$\mathbf{G} = \begin{pmatrix} \mathbf{B} - \eta \mathbf{I}_{N'} & 0 & 0 \\ 0 & \mathbf{D} - \eta \mathbf{I}_M & \eta \mathbf{I}_M \\ 0 & 0 & \mathbf{C} \end{pmatrix}, \quad (11)$$

with \mathbf{B} and \mathbf{D} identical to Eq. (8), \mathbf{C} the coupling matrix of the control network, and η the controlling strength. $\mathbf{I}_{N'}$ and \mathbf{I}_M are identity matrices of dimensions $N' = N - M$ and M , respectively. From Eq. (11) we see that, with the introduction of the control network, the eigenvalues of \mathbf{B} and \mathbf{D} are increased globally by the amount η . In particular, $-\lambda_{\min}$ and λ_1^s are replaced by $-\lambda_{\min} - \eta$ and $-\eta$, respectively. If the cluster-synchronization state is dynamically unstable [e.g., Fig. 2(a1)], the necessary condition for generating cluster synchronization is replaced by $\varepsilon | -\lambda_{\min} - \eta | > \sigma_c$ [Fig. 2(a2)], from which we obtain the critical controlling strength for *inducing* cluster synchronization in the network,

$$\eta > \eta_1 = (\sigma_c / \varepsilon) - \lambda_{\min}. \quad (12)$$

Increasing η further, the modes associated to \mathbf{D} will be shifted rightward [as depicted in Fig. 2(a3)]. As the controllers are coupled to oscillators in the original network in the one-way fashion, the synchronous manifolds therefore is defined by the control network. That is, the modes associated to \mathbf{D} are switched to transverse modes. Once

$$\eta > \eta_2 = \sigma_c / \varepsilon, \quad (13)$$

all the transverse modes, $\{\lambda_{i,i}^t\}$ and $\{\lambda_i^s\}$, will be shifted into the stable region, making the cluster-synchronization state *controlled* to the pattern defined by the control network. If the cluster-synchronization state is topologically unstable [e.g., Fig. 2(b1)], the necessary conditions for inducing and controlling cluster synchronization are still given by Eq. (12) [as depicted in Fig. 2(b2)] and Eq. (13) [as depicted in Fig. 2(b3)], respectively, as the requirement of pattern stability is not changed. We note that the success of generating the topologically unstable pattern lies in the switching of the mode λ_1^s from the synchronous to transverse type. That is, the role of λ_1^s is replaced by the mode λ_1^t of the control network. Here, $0 = \lambda_1^t > \lambda_2^t \geq \dots \geq \lambda_M^t$ are the eigenvalues of \mathbf{C} , which are independent of η .

The above theoretical analysis thus depicts the following picture on the control of unstable synchronous patterns. For $\eta < \eta_1$, there are transverse modes in the unstable region, thus the synchronous pattern is unstable and cannot be generated in the network. Then, as η exceeds η_1 , all the transverse modes are shifted into the stable region and, as a consequence, the synchronous pattern becomes stable and is emerged. Please note that in this case the oscillators within the same cluster are synchronized but not constrained to the controller. It is also worth mentioning that here the dynamics of this synchronous

pattern is identical to that of the control network; i.e., the original network is degenerated to a small-size network which has exactly the same coupling structure as the control network. As a matter of fact, the coupling matrix of the control network [as described by Eq. (2)] is designed based on just such a principle. Finally, as η exceeds η_2 , the synchronous pattern of the original network is constrained to the state of the control network, i.e., the synchronous pattern is controlled. Accompanying this transition, the synchronous manifolds, which are associated to \mathbf{D} when $\eta \in (\eta_1, \eta_2)$, are replaced by the manifolds associated to \mathbf{C} .

IV. APPLICATIONS

To verify the feasibility of the proposed control method, as well as to test the theoretical predictions obtained in Sec. III, we next employ this method to control synchronous patterns in different networks, including a small-size network of apparent symmetries, the Nepal power-grid network, and a realistic network of coupled electronic circuits.

A. Small-size network

We start by applying the control method to control synchronous patterns in a small-size, artificial network. The structure of the network is plotted in Fig. 3(a), which is constructed by a six-node ring network and three nonlocal connections (shortcuts) [21]. To capture the feature of weighted links widely observed in realistic networks, we set $w_{1,4} = 0.8$ for the connection between nodes 1 and 4, and $w = 1$ for the other connections. In simulations, we adopt the chaotic Lorenz oscillator as the nodal dynamics, which is described by equations $(dx/dt, dy/dt, dz/dt)^T = [\alpha(y - x), rx - y - xz, xy - bz]^T$. The parameters of the Lorenz oscillator are chosen as $\alpha = 10$, $r = 35$, and $b = 8/3$, with which the oscillator presents the chaotic motion [46]. The coupling function is chosen as $\mathbf{H}([x, y, z]^T) = [0, x, 0]^T$, i.e., the x variable is coupled to the y variable. Having fixed the nodal dynamics and coupling function, we can obtain the function $\Lambda = \Lambda(\sigma)$ by solving Eq. (10) numerically, which shows that Λ is negative when $\sigma > \sigma_c \approx 8.3$ [45].

For the simple network presented in Fig. 3(a), the network symmetries can be discerned straightforwardly: the reflection symmetries, \mathbf{S}_1 and \mathbf{S}_2 , and the rotation symmetry (of 180°), \mathbf{S}_3 . As discussed in Sec. III, although each symmetry supports potentially a synchronous pattern, only the stable ones are observable. To figure out the stable synchronous patterns numerically, we investigate the variation of the synchronization relationship among the oscillators as a function of the coupling strength, ε . The results are presented in Fig. 3(b). The synchronization relationship is characterized by the synchronization errors $\delta x_i = \langle |x_i - x_2| \rangle$, with $\langle \cdot \rangle$ denoting the time average. Figure 3(b) shows that when $2.6 < \varepsilon < 4.5$, $\delta x_6 = 0$ and $\delta x_3 = \delta x_5$. That is, two synchronous clusters, (2,6) and (3,5), are formed on the network. Clearly, the synchronized nodes satisfy the symmetry \mathbf{S}_1 . [Please note that these two clusters are dependent with each other (i.e., they are generated or disappeared simultaneously on the network), which in Ref. [42] are named as intertwined clusters.] At $\varepsilon \approx 4.5$, $\delta x_i = 0$ for $i = 1, \dots, 6$, indicating that the network is globally synchronized.

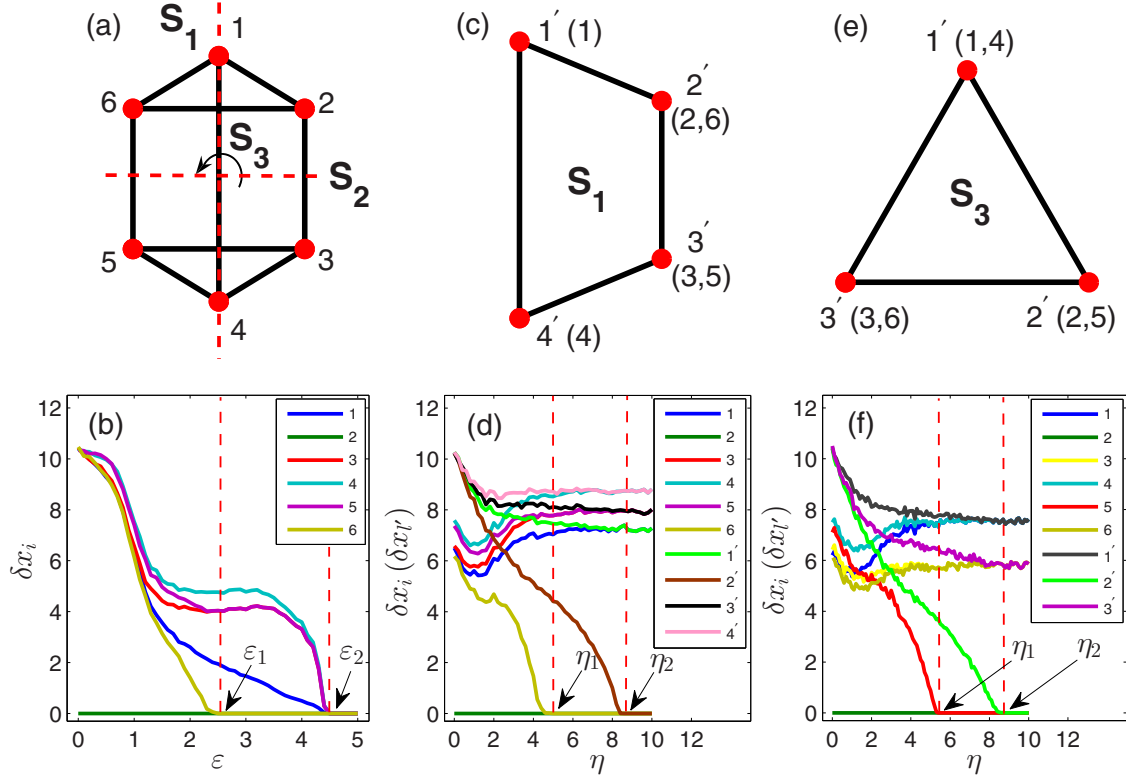


FIG. 3. Controlling synchronous patterns in a six-node network of coupled chaotic Lorenz oscillators. (a) The network structure. The weight of the connection between nodes 1 and 4 is 0.8, and is 1 for the other connections. The network possesses two reflection symmetries, S_1 and S_2 , and one rotation symmetry, S_3 (180° rotation). (b) In the absence of the control network, the synchronization relationship among the oscillators, characterized by the variation of the node synchronization errors $\delta x_i = \langle |x_i - x_2| \rangle$, as a function of the coupling strength, ε . Synchronous pattern associated to S_1 is generated in the region $\varepsilon \in (2.6, 4.5)$. (c) The control network designed according to the symmetry S_1 . Controllers $1'$, $2'$, $3'$, and $4'$ control, respectively, the nodes 1, (2,6), (3,5), and 4. (d) Fixing $\varepsilon = 1.0$, the variation of the synchronization relationship among oscillators (controllers) as a function of the controlling strength, η . The synchronous pattern associated to S_1 is generated (stabilized) for $\eta > \eta_1 \approx 5.0$, and is controlled to the control network for $\eta > \eta_2 \approx 8.6$. (e) The control network designed according to the symmetry S_3 . Controllers $1'$, $2'$, and $3'$ control, respectively, the symmetric pairs (1,4), (2,5), and (3,6). (f) Fixing $\varepsilon = 1.0$, the variation of the synchronization relationship among oscillators (controllers) as a function of η . The synchronous pattern associated to S_3 is generated (stabilized) for $\eta > \eta_1 \approx 5.7$, and is controlled to the control network for $\eta > \eta_2 \approx 8.6$. In (d) and (f), $\delta x_{l'} = \langle |x_{l'} - x_2| \rangle$, with l' the controller index.

We thus infer from Fig. 3(b) that among the three symmetries, only the synchronous pattern associated to S_1 is observable by varying the coupling strength. In what follows, we are going to demonstrate that, with the help of the control network, the synchronous patterns associated to S_2 and S_3 can also be generated when the controlling strength is sufficiently large.

To investigate, we set $\varepsilon = 1.0 < \varepsilon_1$, with which no synchronous cluster is formed on the network. Our first attempt is to generate the synchronous pattern associated to S_1 . (Although this pattern is topologically stable, it is dynamically unstable due to the weak coupling among the oscillators.) Based on the symmetry S_1 , we can construct the control network shown in Fig. 3(c). According to Eq. (2), the coupling matrix of the control network reads

$$\mathbf{C} = \begin{pmatrix} -2.8 & 2 & 0 & 0.8 \\ 1 & -2 & 1 & 0 \\ 0 & 1 & -2 & 1 \\ 0.8 & 0 & 2 & -2.8 \end{pmatrix}. \quad (14)$$

In implementing the control, controllers $1'$, $2'$, $3'$, and $4'$ are coupled unidirectionally to nodes 1, (2,6), (3,5), and 4

in the original network, respectively. By solving Eqs. (3) and (4) numerically, we plot in Fig. 3(d) the variation of the synchronization relationship among the oscillators as a function of the controlling strength, η . Figure 3(d) shows clearly that at $\eta_1 \approx 5.0$, the synchronous pattern associated to S_1 is successfully induced ($\delta x_2 = \delta x_6 = 0$ and $\delta x_3 = \delta x_5$); and, at $\eta_2 \approx 8.6$, the synchronous pattern is controlled to the control network ($\delta x_2 = \delta x_6 = \delta x_{2'} = 0$, $\delta x_3 = \delta x_5 = \delta x_{3'}$, $\delta x_1 = \delta x_{1'}$, and $\delta x_4 = \delta x_{4'}$), i.e., nodes 2 and 6 (nodes 3 and 5) are synchronized to controller $2'$ (controller $3'$).

The critical controlling strengths, η_1 and η_2 , can be analyzed by the theory presented in Sec. III, as follows. Corresponding to the network symmetry S_1 , we have the permutation matrix

$$\mathbf{R} = \begin{pmatrix} 1 & 0 & 0 & 0 & 0 & 0 \\ 0 & 0 & 0 & 0 & 0 & 1 \\ 0 & 0 & 0 & 0 & 1 & 0 \\ 0 & 0 & 0 & 1 & 0 & 0 \\ 0 & 0 & 1 & 0 & 0 & 0 \\ 0 & 1 & 0 & 0 & 0 & 0 \end{pmatrix}, \quad (15)$$

from which we can obtain transformation matrix (constructed by the eigenvectors of \mathbf{R}), which reads

$$\mathbf{T} = \begin{pmatrix} 0 & 0 & 1 & 0 & 0 & 0 \\ 0 & 0.71 & 0 & 0 & 0.71 & 0 \\ -0.71 & 0 & 0 & 0 & 0 & 0.71 \\ 0 & 0 & 0 & 1 & 0 & 0 \\ 0.71 & 0 & 0 & 0 & 0 & 0.71 \\ 0 & -0.71 & 0 & 0 & 0.71 & 0 \end{pmatrix}. \quad (16)$$

The coupling matrix of the original network is

$$\mathbf{W} = \begin{pmatrix} -2.8 & 1 & 0 & 0.8 & 0 & 1 \\ 1 & -3 & -1 & 0 & 0 & 1 \\ 0 & 1 & -3 & 1 & 1 & 0 \\ 0.8 & 0 & 1 & -2.8 & 1 & 0 \\ 0 & 0 & 1 & 1 & -3 & 1 \\ 1 & 1 & 0 & 0 & 1 & -3 \end{pmatrix}, \quad (17)$$

which, after the transformation operation $\mathbf{G} = \mathbf{T}^{-1}\mathbf{W}\mathbf{T}$, has the blocked form as shown in Eq. (8), with

$$\mathbf{B} = \begin{pmatrix} -4 & -1 \\ -1 & -4 \end{pmatrix} \quad (18)$$

and

$$\mathbf{D} = \begin{pmatrix} -2.8 & 0.8 & 1.41 & 0 \\ 0.8 & -2.8 & 0 & 1.41 \\ 1.41 & 0 & -2 & 1 \\ 0 & 1.41 & 1 & -2 \end{pmatrix}. \quad (19)$$

For the matrix \mathbf{B} (which characterizes the transverse spaces of the synchronous pattern), we have the eigenvalues $(\lambda_1^t, \lambda_2^t) = (-3, -5)$; for the matrix \mathbf{D} (which characterizes the synchronous spaces of the synchronous pattern), we have the eigenvalues $(\lambda_1^s, \lambda_2^s, \lambda_3^s, \lambda_4^s) = (0, -1.85, -3, -4.75)$. (Please note that, as (2,6) and (3,5) are intertwined clusters, the matrix \mathbf{B} is not diagonalized [42].) According to Eqs. (12) and (13), we thus have $\eta_1 = (\sigma_c/\varepsilon) - \lambda_{\min} = 8.3 - |\lambda_1^t| = 5.3$ and $\eta_2 = \sigma_c/\varepsilon = 8.3$, which are in good agreement with the numerical results shown in Fig. 3(d).

Our second attempt is to generate the synchronous pattern associated to \mathbf{S}_3 , which, according to the our definitions in Sec. III, is classified as topologically unstable (i.e., $\lambda_{\min} < |\lambda_2^s|$). The control network is presented in Fig. 3(e), in which controllers 1', 2', and 3' are used to control the symmetric pairs (1,4), (2,5), and (3,6), respectively. The coupling matrix of the control network reads

$$\mathbf{C} = \begin{pmatrix} -2 & 1 & 1 \\ 1 & -3 & 2 \\ 1 & 2 & -3 \end{pmatrix}. \quad (20)$$

Figure 3(f) shows the variation of the synchronization relationship of the oscillators as a function of the controlling strength, η . It is seen that when $\eta > \eta_1 \approx 5.7$, $\delta x_1 = \delta_4$, $\delta x_2 = \delta x_6$, and $\delta x_3 = \delta x_5$. That is, the synchronous pattern defined by \mathbf{S}_3 is generated on the network. Increasing η further to $\eta_2 \approx 8.6$, we have $\delta x_{1'} = \delta x_1 = \delta_4$, $\delta x_{2'} = \delta x_2 = \delta x_6$, and $\delta x_{3'} = \delta x_3 = \delta x_5$, i.e., the synchronous pattern is controlled.

Still, the critical controlling strengths, η_1 and η_2 , can be analyzed by the theory presented in Sec. III. For the network

symmetry \mathbf{S}_3 , we have the permutation matrix

$$\mathbf{R} = \begin{pmatrix} 0 & 0 & 0 & 1 & 0 & 0 \\ 0 & 0 & 0 & 0 & 1 & 0 \\ 0 & 0 & 0 & 0 & 0 & 1 \\ 1 & 0 & 0 & 0 & 0 & 0 \\ 0 & 1 & 0 & 0 & 0 & 0 \\ 0 & 0 & 1 & 0 & 0 & 0 \end{pmatrix}. \quad (21)$$

Transforming the coupling matrix \mathbf{W} [Eq. (17)] into the mode space spanned by the eigenvectors of \mathbf{R} , we have the blocked matrix \mathbf{G} [of the form shown in Eq. (8)], with

$$\mathbf{B} = \begin{pmatrix} -3 & 1 & 0 \\ 1 & -3.6 & -1 \\ 0 & -1 & -3 \end{pmatrix}, \quad (22)$$

and

$$\mathbf{D} = \begin{pmatrix} -3 & 2 & 1 \\ 2 & -3 & 1 \\ 1 & 1 & -2 \end{pmatrix}. \quad (23)$$

For the matrix \mathbf{B} , we have the eigenvalues $(\lambda_1^t, \lambda_2^t, \lambda_3^t) = (-1.85, -3, -4.75)$. (Again, the matrix \mathbf{B} is not diagonalized, due to the intertwined clusters [42].) For the matrix \mathbf{D} , we have the eigenvalues $(\lambda_1^s, \lambda_2^s, \lambda_3^s) = (0, -3, -5)$. As $\lambda_{\min} = 1.85 < |\lambda_2^s|$, the synchronous pattern thus is judged as topologically unstable, i.e., it cannot be generated by varying the coupling strength [Fig. 2(b)]. According to the theoretical predications, i.e., Eqs. (12) and (13), we have $\eta_1 = (\sigma_c/\varepsilon) - \lambda_{\min} = 6.4$ and $\eta_2 = \sigma_c/\varepsilon = 8.3$, which agree with the numerical results well [Fig. 3(f)]. (The synchronous pattern associated to \mathbf{S}_2 also can be controlled, with the results similar to that of \mathbf{S}_3 . Here we omit the details for saving the space.)

B. Power-grid network

While the symmetries of a small-size network can be discerned by inspection, the complete set of permutation symmetries of a large-size complex network can only be identified with the help of some sophisticated techniques, e.g., by the tools of computational group theory [36]. Besides, due to the large number of symmetries, the scenario of cluster synchronization in complex network is much more complicated than the small-size ones. For instance, the network may stay on a surprising state where one or more clusters lose synchronization while the remaining clusters are still synchronized, namely the phenomenon of isolated desynchronization [22].

To verify the feasibility of the proposed control method further, we next employ the Nepal power-grid as the network model [47], and investigate the controllability of the synchronous patterns associated to the network symmetries. This may have implications to the functioning of the international (global) power grid [40,41], where the power generators within the same nation are synchronized in both frequency and phase, while the frequency and phase are different among the nations. That is, the functioning of the global grid is based on the synchronous pattern consisting of many synchronized national grids. To make the global grid functioning properly, a crucial issue thus is how to coordinate the synchronous clusters and keep the synchronous pattern stable by some kinds

of central controlling systems. (The similar concerns arise also for the functioning of the interconnection power-grid, where high-voltage direct current lines are used to connect alternating current grids that are not synchronized with each other [48].) The structure of the Nepal power-grid is presented in Fig. 4(a), which consists of 15 nodes (power stations) and 62 links (power lines). For the sake of simplicity, here we treat the network links as nonweighted and nondirected, i.e., $w_{ij} = w_{ji} = 1$. By the technique of computational group theory, we are able to figure out all the network permutation symmetries (totally 86 400), and, according to the permutation orbits, partition the nodes into 5 clusters: $V_1 = \{1,2,3,4,5\}$, $V_2 = \{6,7,8\}$, $V_3 = \{9,10,11,12,13\}$, $V_4 = \{14\}$, and $V_5 = \{15\}$ [22]. Among them, the 4th and 5th clusters are trivial, as each one contains only a single node.

Employing still the chaotic Lorenz oscillator as the nodal dynamics, we plot in Fig. 4(b) the variation of the synchronization relationship among the oscillators as a function of the coupling strength, ε . Here, to better demonstrate the formation of the synchronous clusters, we monitor only the averaged synchronization error of the nontrivial clusters, $\delta\hat{x}_l = \sum_i \langle |x_i - \bar{x}_l| \rangle / n_l$, with $\bar{x}_l = \sum_i x_i / n_l$ the averaged state of the oscillators in cluster l . Clearly, if the l th cluster is synchronized, we have $\delta\hat{x}_l = 0$. Figure 4(b) shows that, with the increase of ε , cluster 1 is first synchronized ($\varepsilon_1 \approx 0.4$), followed by cluster 2 ($\varepsilon_2 \approx 0.8$) and then cluster 3 ($\varepsilon_3 \approx 1.1$). (Please note that different from the case of small-size network, here the clusters are not intertwined.) To exclude the possibility of global network synchronization, we plot in Fig. 4(b) also the variation of the network-averaged synchronization error, $\delta\hat{x}_{\text{net}} = \sum_i \langle |x_i - \bar{x}| \rangle / N$, with $\bar{x} = \sum_i x_i / N$ the network-averaged state. As $\delta\hat{x}_{\text{net}} = 0$ at $\varepsilon_4 \approx 8.9$, we thus confirm that cluster synchronization is generated within the range $\varepsilon \in (\varepsilon_3, \varepsilon_4)$. (Here cluster synchronization refers specifically to the state that all the nontrivial clusters are synchronized. If only part of the clusters are synchronized, we call it the state

of isolated desynchronization [22]. The formation of this state will be discussed later in this section.)

The reference state to be controlled is generated by $\varepsilon = 0.3 < \varepsilon_1$, with which no synchronous cluster is formed on the network. Based on the cluster information, we can construct the control network shown in Fig. 4(c), which consists of 5 controllers and 5 weighted links. According to Eq. (2), we can construct the coupling matrix of the control network as

$$\mathbf{C} = \begin{pmatrix} -3 & 3 & 0 & 0 & 0 \\ 5 & -11 & 5 & 1 & 0 \\ 0 & 3 & -4 & 1 & 0 \\ 0 & 3 & 5 & -9 & 1 \\ 0 & 0 & 0 & 1 & -1 \end{pmatrix}. \quad (24)$$

Controlling the reference state by the scheme proposed in Sec. II, we plot in Fig. 4(d) the variation of the averaged synchronization errors of the nontrivial clusters, $\delta\hat{x}_l$, as a function of the controlling strength, η . It is seen that as η increases, the clusters 2, 3, and 1 are synchronized at $\eta_1 \approx 13$, $\eta_2 \approx 15$, and $\eta_3 \approx 16$, respectively. In particular, in the regime $\eta > \eta_3$, the synchronous pattern, which is unstable without the control, is successfully induced on the network. Increasing η further to $\eta_4 \approx 29$, in Fig. 4(d) it is seen that the synchronous pattern is controlled to the control network, i.e., each synchronous cluster is synchronized to its controller. (The control efficiency is measured by the cluster-controller synchronization errors, $\delta\hat{x}_l = \sum_i \langle |x_i - x_{l'}| \rangle / n_l$, with $x_{l'}$ the state of the controller l' , and $i = 1, \dots, n_l$ the oscillators in cluster l .)

The critical controlling strengths, η_3 and η_4 , can also be analyzed theoretically, based on the method presented in Sec. III. According to the network cluster information, we have the following permutation matrix ($r_{ij} = r_{ji} = 1$ if nodes i and j belong to the same cluster, and $r_{ij} = 0$ otherwise)

$$\mathbf{R} = \begin{pmatrix} 0 & 1 & 1 & 1 & 1 & 0 & 0 & 0 & 0 & 0 & 0 & 0 & 0 & 0 & 0 \\ 1 & 0 & 1 & 1 & 1 & 0 & 0 & 0 & 0 & 0 & 0 & 0 & 0 & 0 & 0 \\ 1 & 1 & 0 & 1 & 1 & 0 & 0 & 0 & 0 & 0 & 0 & 0 & 0 & 0 & 0 \\ 1 & 1 & 1 & 0 & 1 & 0 & 0 & 0 & 0 & 0 & 0 & 0 & 0 & 0 & 0 \\ 1 & 1 & 1 & 1 & 0 & 0 & 0 & 0 & 0 & 0 & 0 & 0 & 0 & 0 & 0 \\ 0 & 0 & 0 & 0 & 0 & 0 & 1 & 1 & 0 & 0 & 0 & 0 & 0 & 0 & 0 \\ 0 & 0 & 0 & 0 & 0 & 1 & 0 & 1 & 0 & 0 & 0 & 0 & 0 & 0 & 0 \\ 0 & 0 & 0 & 0 & 0 & 1 & 1 & 0 & 0 & 0 & 0 & 0 & 0 & 0 & 0 \\ 0 & 0 & 0 & 0 & 0 & 0 & 0 & 0 & 1 & 1 & 1 & 1 & 0 & 0 & 0 \\ 0 & 0 & 0 & 0 & 0 & 0 & 0 & 0 & 1 & 0 & 1 & 1 & 1 & 0 & 0 \\ 0 & 0 & 0 & 0 & 0 & 0 & 0 & 0 & 1 & 1 & 0 & 1 & 1 & 0 & 0 \\ 0 & 0 & 0 & 0 & 0 & 0 & 0 & 0 & 1 & 1 & 1 & 1 & 0 & 0 & 0 \\ 0 & 0 & 0 & 0 & 0 & 0 & 0 & 0 & 0 & 0 & 0 & 0 & 0 & 1 & 0 \\ 0 & 0 & 0 & 0 & 0 & 0 & 0 & 0 & 0 & 0 & 0 & 0 & 0 & 0 & 1 \end{pmatrix}, \quad (25)$$

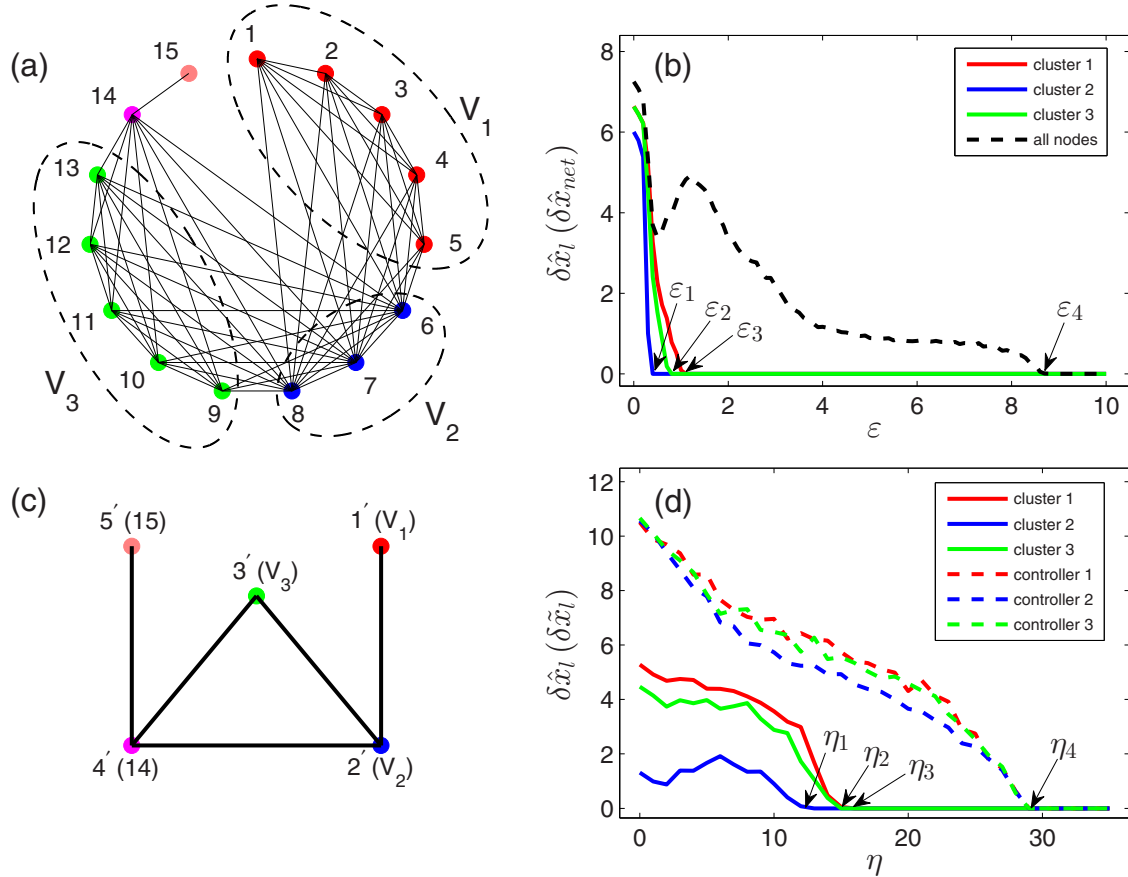


FIG. 4. Controlling synchronous pattern in the Nepal power-grid network. The nodal dynamics and coupling function are the same as described in the caption to Fig. 3. (a) The network structure and the distribution of the clusters. The nodes are partitioned into three nontrivial clusters [$V_1 = \{1,2,3,4,5\}$ (red), $V_2 = \{6,7,8\}$ (blue), and $V_3 = \{9,10,11,12,13\}$ (green)] and two trivial clusters [$V_4 = \{14\}$ (pink) and $V_5 = \{15\}$ (yellow)]. (b) The variations of the cluster synchronization errors, $\delta \hat{x}_l$ with $l = 1,2,3$, and the network synchronization error, $\delta \hat{x}_{net}$, as a function of the coupling strength, ϵ . Clusters 2, 3, and 1 are synchronized at $\epsilon_1 \approx 0.4$, $\epsilon_2 \approx 0.8$, and $\epsilon_3 \approx 1.1$, respectively. For $\epsilon > \epsilon_4 \approx 8.9$, the network is globally synchronized. (c) The control network. Controller l' is coupled unidirectionally to all oscillators in cluster l of the original network. (d) For $\epsilon = 0.3$, the variations of the cluster synchronization errors, $\delta \hat{x}_l$, as a function of the controlling strength, η . Synchronization is induced in clusters 2, 3, and 1 at $\eta_1 \approx 13$, $\eta_2 \approx 15$, and $\eta_3 \approx 16$, respectively. Dashed lines: the variation of the cluster-controller synchronization errors, $\delta \hat{x}_l$, with respect to η . For $\eta > \eta_4 \approx 29$, $\delta \hat{x}_l = 0$, indicating that the synchronous pattern is controlled to the state of the control network.

based on which we can obtain the transformation matrix \mathbf{T} . By \mathbf{T} , we then are able to transform the coupling matrix into the blocked form, with

$$\mathbf{B} = \begin{pmatrix} -8 & 0 & 0 & 0 & 0 & 0 & 0 & 0 & 0 & 0 & 0 \\ 0 & -8 & 0 & 0 & 0 & 0 & 0 & 0 & 0 & 0 & 0 \\ 0 & 0 & -8 & 0 & 0 & 0 & 0 & 0 & 0 & 0 & 0 \\ 0 & 0 & 0 & -8 & 0 & 0 & 0 & 0 & 0 & 0 & 0 \\ 0 & 0 & 0 & 0 & -14 & 0 & 0 & 0 & 0 & 0 & 0 \\ 0 & 0 & 0 & 0 & 0 & -14 & 0 & 0 & 0 & 0 & 0 \\ 0 & 0 & 0 & 0 & 0 & 0 & -9 & 0 & 0 & 0 & 0 \\ 0 & 0 & 0 & 0 & 0 & 0 & 0 & -9 & 0 & 0 & 0 \\ 0 & 0 & 0 & 0 & 0 & 0 & 0 & 0 & -9 & 0 & 0 \\ 0 & 0 & 0 & 0 & 0 & 0 & 0 & 0 & 0 & -9 & 0 \\ 0 & 0 & 0 & 0 & 0 & 0 & 0 & 0 & 0 & 0 & -9 \end{pmatrix}, \quad (26)$$

and

$$\mathbf{D} = \begin{pmatrix} -9 & 1 & 1.73 & 0 & 2.24 \\ 1 & -1 & 0 & 0 & 0 \\ 1.73 & 0 & -11 & 3.87 & 3.87 \\ 0 & 0 & 3.87 & -3 & 0 \\ 2.24 & 0 & 3.87 & 0 & -4 \end{pmatrix}. \quad (27)$$

From the matrix \mathbf{B} we have $\lambda_{\min} = 8$, which, according to Eq. (12), gives the critical controlling strength for inducing the synchronous pattern, $\eta_3 \approx 20$. Meanwhile, according to Eq. (13), we also have the critical controlling strength for controlling the synchronous pattern, $\eta_4 \approx 28$. As depicted in Fig. 4(d), these theoretical results agree well with the numerical results.

Besides the critical strengths η_3 and η_4 , the other two critical controlling strengths observed in numerical simulations, i.e., η_1 and η_2 , can also be analyzed. Noticing that \mathbf{B} can be rewritten in the blocked form

$$\mathbf{B} = \begin{pmatrix} \mathbf{B}_1 & 0 & 0 \\ 0 & \mathbf{B}_2 & 0 \\ 0 & 0 & \mathbf{B}_3 \end{pmatrix}, \quad (28)$$

with \mathbf{B}_l the transverse space of the l th (nontrivial) cluster. [Please note that for the general complex networks, the matrix \mathbf{B} has the blocked form shown in Eq. (28). But for the specific network of Nepal power-grid, \mathbf{B} is diagonal.] According to the scenario of cluster synchronization depicted in Fig. 2, the l th cluster is synchronized when $\sigma_{l,1} = \varepsilon |\lambda_{l,1}^t| > \sigma_c$, with $\lambda_{l,1}^t$ the largest eigenvalue of \mathbf{B}_l . When control is added, $\lambda_{l,1}^t$ is replaced by $\lambda_{l,1}^t - \eta$ (as analyzed in Sec. III). The condition for cluster synchronization thus becomes $\varepsilon |\lambda_{l,1}^t - \eta| > \sigma_c$. That is, to make the l th cluster synchronizable (despite the synchronization relationship of the remaining oscillators), the controlling strength should be larger to

$$\eta_l = (\sigma_c / \varepsilon - |\lambda_{l,1}^t|). \quad (29)$$

For the matrices \mathbf{B}_2 and \mathbf{B}_3 in Eq. (28), we have $\lambda_{1,1}^t = -14$ and $\lambda_{2,1}^t = -9$, respectively. According to Eq. (29), we thus have $\eta_1 = 14$ (cluster 1 is synchronized) and $\eta_2 = 19$ (cluster 2 is synchronized), which agree with the numerical results very well (numerically we have $\eta_1 \approx 13$ and $\eta_2 \approx 15$).

From the viewpoint of practical applications, a commonly interested issue is the dependence the critical controlling strength, η_4 , on the system coupling strength, ε , as both quantities reflect the cost for generating the desired synchronous pattern. To investigate, we plot in Fig. 5 the variation of η_4 as a function of the normalized coupling strength, $\varepsilon/\varepsilon_4$, with $\varepsilon_4 = 8.9$ the critical coupling strength for generating global synchronization [see Fig. 4(b)]. It is seen in Fig. 5 that, as the coupling strength increases, the value of η_4 is gradually decreased. That is, the stronger the coupling among the oscillators is, the smaller is the strength needed to control the network to the desired pattern. A fitting of the numerical data shows that $\eta \propto 1/\varepsilon$, which is exactly what we have obtained by the method of eigenvalue analysis [i.e., Eq. (13)].

C. Experimental demonstration

Can synchronous patterns be controlled in realistic systems? In our theoretical and numerical studies, it is assumed that the nodal dynamics is identical and the network structure is of perfect symmetry. In a realistic situation, parameter mismatch and noise perturbations are unavoidable. To check the feasibility of the control method to realistic networks, we finally investigate the control of cluster synchronization in network of coupled electronic circuits. Specifically, we adopt still the network structure of Fig. 3(a), but employ

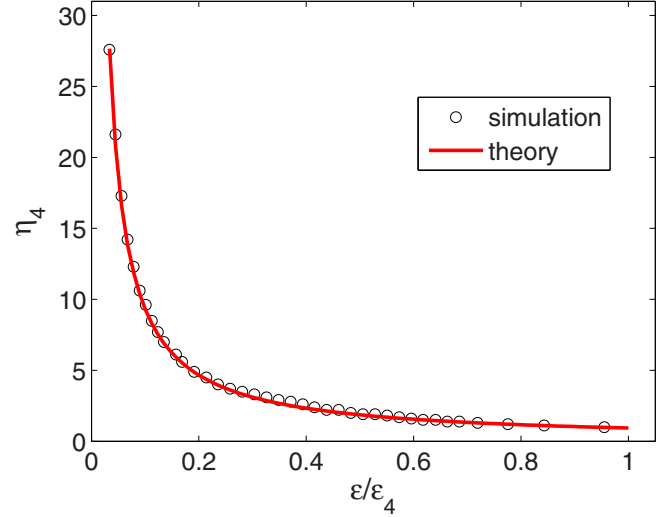


FIG. 5. For the Nepal power-grid network, the variation of the critical controlling strength for pattern control, η_4 , as a function of the normalized coupling strength, $\varepsilon/\varepsilon_4$, with ε_4 the critical coupling strength for global synchronization [see Fig. 4(b)]. Open circles: the numerical results. Solid line: the theoretical results given by Eq. (13).

the Hindmarsh-Rose (HR) neuronal circuit as the nodal dynamics [49,50]. The HR circuit is described by equations

$$\begin{aligned} \dot{x} &= y - ax^3 + bx^2 - z + I_e, \\ \dot{y} &= c - dx^2 - y, \\ \dot{z} &= r[s(x + 1.6) - z], \end{aligned} \quad (30)$$

with (a, b, c, d, r, s) the system parameters, and I_e the external forcing current. This model has been widely employed in literature for modeling the firing activities of neurons, and its experimental realizations by electronic circuits have been well designed and investigated. Here, we adopt the circuit diagram designed in Ref. [50] and couple the circuits through the x variable, i.e., $\mathbf{H}([x, y, z]^T) = [x, 0, 0]^T$. We set the system parameters as $(a, b, c, d, r, s) = (1, 3, 1, 5, 6 \times 10^{-3}, 4)$, and choose the external current $I_e = 320 \mu\text{A}$, with which the circuit shows the chaotic motion [49]. The whole experimental process is controlled and monitored by the virtual interface of the software MULTISIM 12.0.

To demonstrate, we choose Fig. 3(e) as the control network. That is, we are trying to control the network to the synchronous pattern associated to \mathbf{S}_3 , which, according to the eigenvalue analysis, is topologically unstable [Fig. 2(b)]. We fix the coupling strength among the circuits in the original network as $\varepsilon = 1.53$, with which no synchronization is observed between any two circuits. Using this nonsynchronous state as the reference state, we activate the control and record the synchronization relationship among the circuits under different controlling strengths, η . The typical results are plotted in Fig. 6. When η is too weak, e.g., $\eta = 1.0$ in Fig. 6(a), it is seen that the circuits in the original network are neither synchronized in pairs [Fig. 6(a1)] nor controlled to their corresponding controllers [Fig. 6(a2)]. Increasing the controlling strength to $\eta = 4.5$ [Fig. 6(b)], it is seen that circuits 1, 2, and 3 are synchronized with circuits 4, 5, and 6, respectively,

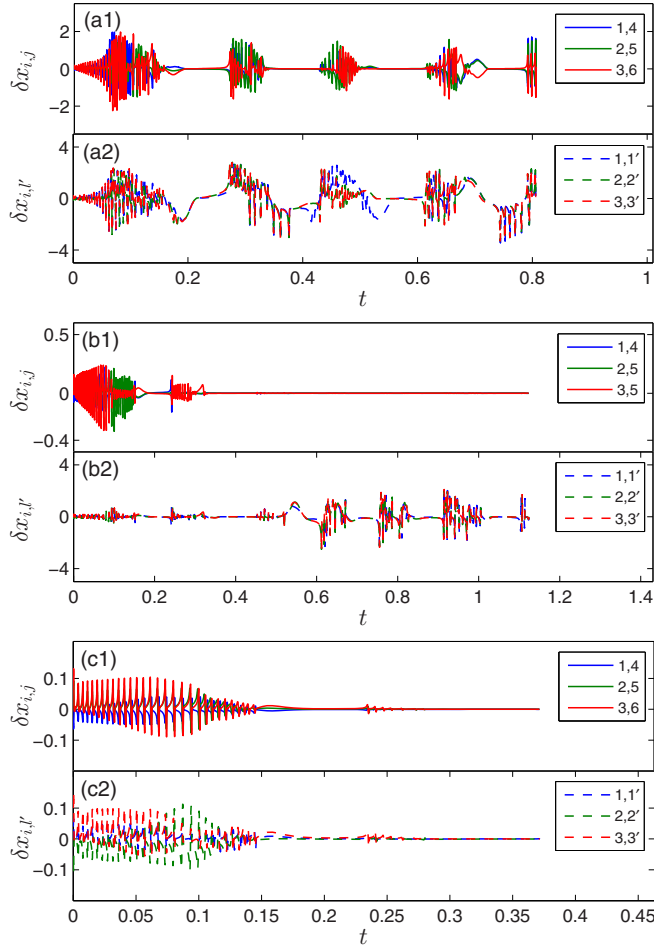


FIG. 6. Experimental demonstrations on the control of synchronous pattern in network of coupled chaotic HR circuits. The network structure is the same as described in the caption to Fig. 3(a), and the coupling strength is fixed as $\varepsilon = 1.53$. The control network is the same as described in the caption to Fig. 3(e). The variations of the synchronization relationship among the oscillators (controllers) for different controlling strengths. (a) $\eta = 1.0$. No synchronous cluster is formed. (b) $\eta = 4.5$. Cluster synchronization is induced but is not controlled. (c) $\eta = 6.9$. Cluster synchronization is both induced and controlled. $\delta \mathbf{x}_{i,j} = \mathbf{x}_i - \mathbf{x}_j$ denotes the synchronization error between circuits i and j . $\delta \mathbf{x}_{i,l'} = \mathbf{x}_i - \mathbf{x}_{l'}$ denotes the control error between circuit i and controller l' .

i.e., the cluster-synchronization state is induced [Fig. 6(b1)]. However, as depicted in Fig. 6(b2), the synchronized pairs are not controlled to their corresponding controllers, i.e., the cluster-synchronization state is not controlled. Increasing η further to 6.9 [Fig. 6(c)], it is seen that not only the cluster-synchronization state is induced in the original network [Fig. 6(c1)], but also it is controlled to the state of the control network [Fig. 6(c2)].

For the HR circuits described by Eq. (30), numerically we find that the largest Lyapunov exponent of the MSF curve is negative in the regime $\sigma > \sigma_c \approx 9.5$. As the structures of the original and control networks are the same as described in the captions to Figs. 3(a) and 3(e), the eigenvalues of the transverse and synchronous modes therefore are also given by Eqs. (22) and (23), respectively. According to the

theoretical predications, i.e., Eqs. (12) and (13), we thus have $\eta_1 \approx 4.4$ (for inducing cluster synchronization) and $\eta_2 \approx 6.2$ (for controlling cluster synchronization). As depicted in Fig. 6, these theoretical predications agree with the experimental results very well.

V. DISCUSSIONS AND CONCLUSION

We would like to make the following remarks. First, the current study is inspired by the recent progress of cluster synchronization in complex networks [15–22]. In particular, in Ref. [22] the authors have proposed a numerical method for identifying the topological clusters, which paves the way to the investigation of cluster synchronization in large-size complex networks. However, different from previous studies, which emphasize the emergence of cluster synchronization by varying the coupling strength, here we focus on how to control the unstable cluster-synchronization states by an elaborately designed small-size network. As we have argued and demonstrated, with the help of the control network, not only the dynamically unstable patterns can be generated on the network, but also the topologically unstable ones. Regarding the significance of synchronous patterns to the functioning of many realistic complex networks, e.g., the neuronal network and the global grid, the control method proposed in the present work may have broad applications.

Second, the present work is essentially different from the existing studies of controlling network synchronization. In parallel with the investigations of network synchronization, in the past years considerable attentions have been also given to the synchronization of complex networks driven by an externally added controller, namely the scheme of pinning synchronization [51–53]. In the general picture of pinning synchronization, a controller, which has the identical dynamics as the network node, is coupled to some of the network nodes unidirectionally (pinning coupling), and the central task there is to control the network to the *uniform* state of global synchronization [51–53]. As the controller has the same dynamics and coupling function as the network nodes, the study of pinning synchronization is essentially a problem of global synchronization if treating the controller as an additional node to the existing network. Different from pinning synchronization, in our present work the control network itself is a spatially extended system, which is designed according to the network symmetries. To control the network to different synchronous patterns, different control networks should be designed. More importantly, in this new control scheme the targeting state is spatially *nonuniform*, i.e., the synchronous pattern, instead of the uniform state of global synchronization. For this difference, the stability analysis of cluster synchronization is also essentially different from that of pinning (global) synchronization, as has been discussed in Sec. III.

Third, the proposed method might be also used to control the chimera-like synchronization states [54,55]. This interesting state can be observed in Fig. 4(b) in the range $\varepsilon \in (\varepsilon_1, \varepsilon_2)$, where only the nodes within the first cluster are synchronized, while the remaining nodes in the network are desynchronized. As such, the synchronous and nonsynchronous motions coexist in the network. This feature is very similar to that of the chimera state observed recently in

the lattices of coupled periodic oscillators [54,55] and is named isolated desynchronization in Ref. [22]. As depicted in Fig. 2, the isolated-desynchronization state could be unstable, due to either the weak coupling strength [Fig. 2(a)] or the network structure [Fig. 2(b)]. To control the isolated-desynchronization states, we can simply replace the control network by a single controller and couple it unidirectionally to all nodes within the targeting cluster. The stability analysis will be identical to that of cluster synchronization given in Sec. II, except that the synchronous manifold is now defined by the controller, and only the transverse modes of the targeting cluster are concerned.

Finally, the proposed control method is expected as applicable to the general complex network. As the underlying mechanism of pinning control is governed by synchronization, the proposed control method, in principle, can be applied to the general network showing synchronization behaviors. Besides, after some modifications, the control method could be also used to control cluster synchronization in complex networks consisting of nonidentical oscillators. This idea is inspired by the isolated-desynchronization state described above [22], where a synchronous cluster appeared on the desynchronization background. Given that nodes within the same cluster are of identical dynamics, the network symmetry will still be satisfied, and the same control method will be applied. In realistic situations, time delay is unavoidable in signal propagating and processing, which may influence the stability of the synchronous patterns. Our preliminary results show that given the time delay is small enough (e.g., smaller to 3×10^{-2} in networked Lorenz oscillators), synchronous

patterns can still be successfully induced and controlled. We hope to solidify the idea of nonidentical oscillators and conduct a detail analysis on the impacts of time delay on synchronous patterns in our future studies.

In summary, we have proposed a general framework for controlling synchronous patterns in symmetric complex networks. We have given the details on how to design the control network based on the information of the network symmetries, analyzed the underlying mechanism for this control method, and obtained explicitly the formula for the critical controlling strengths. The efficiency of the control method has been justified by numerical simulations of both artificial and realistic network models, and demonstrated by realistic experiment of networked electric circuits. Our studies highlight the controllability of synchronous patterns in complex networks, which might be helpful to our understanding of the functioning of some realistic complex systems, e.g., the DA complex [38,39], and to the design of modern control techniques, e.g., the management of the global power grid [40,41].

ACKNOWLEDGMENTS

The authors thank Dr. Mengjiao Chen for helpful discussions. This work was supported by the National Natural Science Foundation of China under Grants No. 11375109 and No. 11274271. X.G.W. was also supported by the Fundamental Research Funds for the Central Universities under Grant No. GK201601001.

-
- [1] Y. Kuramoto, *Chemical Oscillations, Waves, and Turbulence* (Springer, Berlin, 1984).
 - [2] A. S. Pikovsky, M. G. Rosenblum, and J. Kurths, *Synchronization: A Universal Concept in Nonlinear Science* (Cambridge University Press, Cambridge, 2001).
 - [3] S. Strogatz, *Sync: The Emerging Science of Spontaneous Order* (Hyperion, New York, 2003).
 - [4] S. Boccaletti, V. Latora, Y. Moreno, M. Chavez, and D.-U. Hwang, Complex networks: Structure and dynamics, *Phys. Rep.* **424**, 175 (2006).
 - [5] A. Arenas, A. Diaz-Guilera, J. Kurths, Y. Moreno, and C. S. Zhou, Synchronization in complex networks, *Phys. Rep.* **469**, 93 (2008).
 - [6] L. M. Pecora and T. L. Carroll, Synchronization in Chaotic Systems, *Phys. Rev. Lett.* **64**, 821 (1990).
 - [7] X. G. Wang, L. Huang, S. G. Guan, Y.-C. Lai, and C.-H. Lai, Onset of synchronization in complex gradient networks, *Chaos* **18**, 037117 (2008).
 - [8] A. E. Motter, S. A. Myers, M. Anghel, and T. Nishikawa, Spontaneous synchrony in power-grid networks, *Nat. Phys.* **9**, 191 (2013).
 - [9] E. R. Kandel, J. H. Schwartz, and T. M. Jessell, *Principles of Neural Science* (McGraw-Hill, New York, 2000).
 - [10] E. Basar, *Brain Function and Oscillation* (Springer, New York, 1998).
 - [11] V. N. Belykh and E. Mosekilde, One-dimensional map lattices: Synchronization, bifurcations, and chaotic structures, *Phys. Rev. E* **54**, 3196 (1996).
 - [12] M. Hasler, Yu. Maistrenko, and O. Popovych, Simple example of partial synchronization of chaotic systems, *Phys. Rev. E* **58**, 6843 (1998).
 - [13] Y. Zhang, G. Hu, H. A. Cerdeira, S. Chen, T. Braun, and Y. Yao, Partial synchronization and spontaneous spatial ordering in coupled chaotic systems, *Phys. Rev. E* **63**, 026211 (2001).
 - [14] A. Pikovsky, O. Popovych, and Yu. Maistrenko, Resolving Clusters in Chaotic Ensembles of Globally Coupled Identical Oscillators, *Phys. Rev. Lett.* **87**, 044102 (2001).
 - [15] B. Ao and Z. G. Zheng, Partial synchronization on complex networks, *Europhys. Lett.* **74**, 229 (2006).
 - [16] C. S. Zhou and J. Kurths, Hierarchical synchronization in complex networks with heterogeneous degrees, *Chaos* **16**, 015104 (2006).
 - [17] F. Sorrentino, and E. Ott, Network synchronization of groups, *Phys. Rev. E* **76**, 056114 (2007).
 - [18] T. Dahms, J. Lehnert, and E. Schöll, Cluster and group synchronization in delay-coupled networks, *Phys. Rev. E* **86**, 016202 (2012).
 - [19] V. Nicosia, M. Valencia, M. Chavez, A. Diaz-Guilera, and V. Latora, Remote Synchronization Reveals Network Symmetries and Functional Modules, *Phys. Rev. Lett.* **110**, 174102 (2013).

- [20] C. Fu, Z. Deng, L. Huang, and X. G. Wang, Topological control of synchronous patterns in systems of networked chaotic oscillators, *Phys. Rev. E* **87**, 032909 (2013).
- [21] C. Fu, W. Lin, L. Huang, and X. G. Wang, Synchronization transition in networked chaotic oscillators: The viewpoint from partial synchronization, *Phys. Rev. E* **89**, 052908 (2014).
- [22] L. M. Pecora, F. Sorrentino, A. M. Hagerstrom, T. E. Murphy, and R. Roy, Cluster synchronization and isolated desynchronization in complex networks with symmetries, *Nat. Commun.* **5**, 4079 (2014).
- [23] F. Sorrentino, L. M. Pecora, A. M. Hagerstrom, T. E. Murphy, and R. Roy, Complete characterization of stability of cluster synchronization in complex dynamical networks, [arXiv:1507.04381](https://arxiv.org/abs/1507.04381).
- [24] D. J. Watts and S. H. Strogatz, Collective dynamics of small-world networks, *Nature (London)* **393**, 440 (1998).
- [25] A.-L. Barabási and R. Albert, Emergence of scaling in random networks, *Science* **286**, 509 (1999).
- [26] P. M. Gade and C.-K. Hu, Synchronous chaos in coupled map lattices with small-world interactions, *Phys. Rev. E* **62**, 6409 (2000).
- [27] M. Barahona and L. M. Pecora, Synchronization in Small-World Systems, *Phys. Rev. Lett.* **89**, 054101 (2002).
- [28] T. Nishikawa, A. E. Motter, Y.-C. Lai, and F. C. Hoppensteadt, Heterogeneity in Oscillator Networks: Are Smaller Worlds Easier to Synchronize? *Phys. Rev. Lett.* **91**, 014101 (2003).
- [29] A. E. Motter, C. Zhou, and J. Kurths, Weighted networks are more synchronizable: How and why, *AIP Conf. Proc.* **776**, 201 (2005).
- [30] K. Park, L. Huang, and Y.-C. Lai, Desynchronization waves in small-world networks, *Phys. Rev. E* **75**, 026211 (2007).
- [31] X. G. Wang, S. Guan, Y.-C. Lai, B. Li, and C. H. Lai, Desynchronization and on-off intermittency in complex networks, *Europhys. Lett.* **88**, 28001 (2009).
- [32] C. Fu, H. Zhang, M. Zhan, and X. G. Wang, Synchronous patterns in complex systems, *Phys. Rev. E* **85**, 066208 (2012).
- [33] O. D’Huys, R. Vicente, T. Erneux, J. Danckaert, and I. Fischer, Synchronization properties of network motifs: Influence of coupling delay and symmetry, *Chaos* **18**, 037116 (2008).
- [34] G. Russo and J. J. E. Slotine, Symmetries, stability, and control in nonlinear systems and networks, *Phys. Rev. E* **84**, 041929 (2011).
- [35] M. Golubitsky and I. Stewart, Recent advances in symmetric and network dynamics, *Chaos* **25**, 097612 (2015).
- [36] W. Stein, *SAGE: Software for Algebra an Geometry Experimentation* (2013) <http://www.sagemath.org/sage/>.
- [37] B. D. MacArthur and R. J. Sanchez-Garcia, and J. W. Anderson, On automorphism groups of networks, *Discrete Appl. Math.* **156**, 3525 (2008).
- [38] R. Andersson, A. Johnston, and A. Fisahn, Dopamine D4 receptor activation increases hippocampal gamma oscillations by enhancing synchronization of fast-spiking interneurons, *PLoS ONE* **7**, e40906 (2012).
- [39] L. Yetnikoff, H. N. Lavezzi, R. A. Reichard, and D. S. Zahm, An update on the connections of the ventral mesencephalic dopaminergic complex, *Neuroscience* **282**, 23 (2014).
- [40] M. Z. Jacobson and M. A. Delucchi, Providing all global energy with wind, water, and solar power, Part I: Technologies, energy resources, quantities and areas of infrastructure, and materials, *Energy Policy* **39**, 1154 (2011).
- [41] S. Chatzivasilieadis, D. Ernst, and G. Andersson, The global grid, *Renewable Energy* **57**, 372 (2013).
- [42] L. M. Pecora and T. L. Carroll, Synchronization of chaotic systems, *Chaos* **25**, 097611 (2015).
- [43] L. M. Pecora and T. L. Carroll, Master Stability Functions for Synchronized Coupled Systems, *Phys. Rev. Lett.* **80**, 2109 (1998).
- [44] G. Hu, J. Z. Yang, and W. Liu, Instability and controllability of linearly coupled oscillators: Eigenvalue analysis, *Phys. Rev. E* **58**, 4440 (1998).
- [45] L. Huang, Q. Chen, Y.-C. Lai, and L. M. Pecora, Generic behavior of master-stability functions in coupled nonlinear dynamical systems, *Phys. Rev. E* **80**, 036204 (2009).
- [46] E. N. Lorenz, Deterministic nonperiodic flow, *J. Atmos. Sci.* **20**, 130 (1963).
- [47] Nepal electricity authority annual report 2011, www.nea.org.np (2011).
- [48] M. P. Bahrman and B. K. Johnson, The ABCs of HVDC transmission technologies, *IEEE Power & Energy Magazine* **5**, 32 (2007).
- [49] J. L. Hindmarsh and R. M. Rose, A model of neuronal bursting using three coupled first order differential equations, *Proc. R. Soc. London B* **221**, 87 (1984).
- [50] G. Ren, J. Tang, J. Ma, and Y. Xu, Detection of noise effect on coupled neuronal circuits, *Commun. Nonlinear Sci. Numer. Simulat.* **29**, 170 (2015).
- [51] X. F. Wang and G. R. Chen, Pinning control of scale-free dynamical networks, *Physica A* **310**, 521 (2002).
- [52] F. Sorrentino, M. di Bernardo, F. Garofalo, and G. R. Chen, Controllability of complex networks via pinning, *Phys. Rev. E* **75**, 046103 (2007).
- [53] L. Yang, X. G. Wang, Y. Li, and Z. M. Sheng, On the pinning strategy of complex networks, *Europhys. Lett.* **92**, 48002 (2010).
- [54] Y. Kuramoto and D. Battogtokh, Coexistence of coherence and incoherence in nonlocally coupled phase oscillators, *Nonlinear Phenom. Complex Syst.* **5**, 380 (2002).
- [55] D. M. Abrams and S. H. Strogatz, Chimera States for Coupled Oscillators, *Phys. Rev. Lett.* **93**, 174102 (2004).